Preliminary Study of Ai-assisted Diagnosis Using FDG-PET/CT for Axillary Lymph Node Metastasis in Patients With Breast Cancer

Zongyao Li
Hokkaido University
Kazuhiro Kitajima
Hyogo College of Medicine
Kenji Hirata (✉ khirata@med.hokudai.ac.jp)
Department of Diagnostic Imaging, Hokkaido University, Kita 15, Nishi 7, Kita-Ku, Sapporo, Hokkaido 060-8638, Japan. https://orcid.org/0000-0003-0036-8975
Ren Togo
Hokkaido University
Junki Takenaka
Hokkaido University
Yasuo Miyoshi
Hyogo College of Medicine
Kohsuke Kudo
Hokkaido University
Takahiro Ogawa
Hokkaido University
Miki Haseyama
Hokkaido University

Original research

Keywords: breast cancer, axillary lymph node, FDG-PET/CT, AI-assisted diagnosis, deep convolutional neural network

Posted Date: October 21st, 2020

DOI: https://doi.org/10.21203/rs.3.rs-93286/v1

Version of Record: A version of this preprint was published on January 25th, 2021. See the published version at https://doi.org/10.1186/s13550-021-00751-4.

Original Research Article

Preliminary study of AI-assisted diagnosis using FDG-PET/CT for axillary lymph node metastasis in patients with breast cancer

Authors:

Zongyao Li,[1] Kazuhiro Kitajima,[2] Kenji Hirata,[3] Ren Togo,[4] Junki Takenaka,[3] Yasuo Miyoshi,[5] Kohsuke Kudo,[3,6] Takahiro Ogawa,[7] Miki Haseyama[7]

Affiliations:

[1]Graduate School of Information Science and Technology, Hokkaido University, N-14, W-9, Kita-ku, Sapporo 060-0814, Japan

[2]Department of Radiology, Division of Nuclear Medicine and PET Center, Hyogo College of Medicine, 1-1 Mukogawa-cho, Nishinomiya, Hyogo 663-8501, Japan

[3]Department of Diagnostic Imaging, Graduate School of Medicine, Hokkaido University, N-15, W-7, Kita-ku, Sapporo 060-8638, Japan

[4]Education and Research Center for Mathematical and Data Science, Hokkaido University, N-12, W-7, Kita-ku, Sapporo 060-0812, Japan

[5]Department of Breast and Endocrine Surgery, Hyogo College of Medicine, 1-1 Mukogawa-cho, Nishinomiya, Hyogo, 663-8501, Japan

[6]Global Center for Biomedical Science and Engineering, Faculty of Medicine, Hokkaido University, N-14, W-9, Kita-ku, Sapporo, 060-0814, Japan

[7]Faculty of Information Science and Technology, Hokkaido University, N-14, W-9, Kita-ku, Sapporo, 060-0814, Japan

*Corresponding author: Dr. Kenji Hirata, Department of Diagnostic Imaging, Hokkaido University, Kita 15, Nishi 7, Kita-Ku, Sapporo, Hokkaido 060-8638, Japan.

Tel.: +81-11-706-7779. Email: khirata@med.hokudai.ac.jp

ABSTRACT

Background: To improve the diagnostic accuracy of axillary lymph node (LN) metastasis in breast cancer patients using FDG-PET/CT, we constructed an artificial intelligence (AI)-assisted diagnosis system that uses deep-learning technologies.

Materials and Methods: Two clinicians and the new AI system retrospectively analyzed and diagnosed 414 axillae of 407 patients with biopsy-proven breast cancer who had undergone FDG-PET/CT before a mastectomy or breast-conserving surgery with a sentinel lymph node (LN) biopsy and/or axillary LN dissection. We designed and trained a deep 3D convolutional neural network (CNN) as the AI model. The diagnoses from the clinicians were blended with the diagnoses from the AI model to improve the diagnostic accuracy.

Results: Although the AI model did not outperform the clinicians, the diagnostic accuracies of the clinicians were considerably improved by collaborating with the AI model: the two clinicians' sensitivities of 59.8% and 57.4% increased to 68.6% and 64.2%, respectively, whereas the clinicians' specificities of 99.0% and 99.5% remained unchanged.

Conclusions: It is expected that AI using deep-learning technologies will be useful in diagnosing axillary LN metastasis using FDG-PET/CT. Even if the diagnostic performance of AI is not better than that of clinicians, taking AI diagnoses into consideration may positively impact the overall diagnostic accuracy.

Keywords: breast cancer, axillary lymph node, FDG-PET/CT, AI-assisted diagnosis, deep convolutional neural network

Background

Breast cancer has been reported as the most prevalent cancer among women in western countries, and it causes the second greatest number of cancer-related deaths among females [1]. The treatments and prognoses of breast cancer depend on several factors including the size and grade of the tumor, the patient's endocrine (hormonal) receptor (ER) status and human epidermal growth factor receptor 2 (HER2) status, axillary lymph node (LN) involvement, and metastatic spread. Among these factors, the extent of axillary LN metastasis is regarded as the most reliable predictor of survival in breast cancer [2]. A determination of the patient's axillary nodal status before treatment can contribute to management decisions and is thus significant.

The 'gold standard' for diagnosing axillary LN involvement is a pathological examination of aspiration cytology, a sentinel LN biopsy (SLNB), and an axillary LN dissection (ALND); however, these are invasive methods. In contrast, the utility of noninvasive ^{18}F-fluorodeoxyglucose positron emission tomography/computed tomography (FDG-PET/CT) for the diagnosis of axillary LN metastasis in patients with breast cancer has been described by several research groups [3–9], one of which achieved a relatively low pooled sensitivity value of 60% and a quite high pooled specificity value of 97% [8].

To improve the accuracy of diagnoses of axillary LN metastasis by clinicians using FDG-PET/CT, recent artificial intelligence (AI) technologies are worthy of consideration. Deep learning technologies, which typically use deep convolutional neural networks (DCNNs), have been widely applied to the field of medical image analysis [10], including FDG-PET/CT [11]. Although AI models trained with mass data can be competitive with experienced clinicians in some applications, in most cases, AI cannot outperform clinicians. This is due in part to the lack of well-annotated data. However, suboptimal AI models trained with a limited amount of data may not necessarily be useless.

In this study, we examined the practicability of using deep-learning technologies to improve the diagnosis of axillary LN metastasis with FDG-PET/CT for breast cancer patients. We constructed an AI-assisted diagnosis system by developing a DCNN-based diagnosis method and a collaboration method blending AI and clinicians' diagnoses. The experimental results confirmed the effectiveness of the proposed AI-assisted diagnosis using deep-learning technologies.

Materials and Methods

Patients

The appropriate review board at each institution approved this retrospective study, and the requirement for patient-informed consent was waived. We collected the data of 410 female patients with newly diagnosed invasive breast cancer who underwent pretreatment whole-body FDG-PET/CT examinations before their surgery between September 2008 and September 2019. We excluded three patients with other existing diseases (malignant lymphoma, leukemia, and sarcoidosis). Seven patients had bilateral breast cancer, and thus a final total of 414 index breast cancers in 407 patients (28–90 years; mean±SD 59.2±14.0 years) were included in the study. The patient and tumor characteristics are summarized in Table 1. One hundred twenty-five patients (30.7%) underwent neoadjuvant chemotherapy (NAC) and/or hormonal therapy before the surgery. For the NAC, anthracycline-containing regimens, anthracycline followed by taxanes, or taxane-based regimens were administered. Hormonal therapy was given to the patients with hormone receptor-positive breast cancer, and the patients with HER2-positive breast cancer were treated with a trastuzumab-based regimen.

The subtypes of the 414 tumors were luminal A (ER+/HER2−, Ki67 <20%) in 148 tumors (14.3%), luminal B (ER+/HER2−, Ki67 ≥20%) in 120 (35.7%) tumors, luminal-HER2 (ER+/HER2+) in 43 (10.4%) tumors, HER2-positive (non-luminal) in 43 (10.4%) tumors, and triple-negative in 60 (14.5%) tumors. Regarding the tumor-node-metastasis (TNM) stage, the tumors of 140 patients (33.8%) were stage I, those of 217 (52.4%) were stage II, and those of the other 57 (13.8%) were stage III.

Among the 414 axillae, 204 (49.3%) were diagnosed pathologically as having axillary LN metastasis. The axillary node metastasis was confirmed by the overall assessment of aspiration cytology, SLNB, and ALND. Histopathologic characteristics were determined based on the samples obtained by core needle biopsy and surgical resection findings.

FDG-PET/CT

All FDG-PET/CT examinations were performed by using one of four PET/CT scanners: a Gemini GXL (Philips Medical Systems, Eindhoven, The Netherlands) (n=283), Gemini TF (Philips Medical Systems) (n=72), Ingenuity TF (Philips Medical Systems) (n=26), and Discovery IQ5 (GE Healthcare, Waukesha, WI, USA) (n=26). The clinical parameters are shown in Table 2.

Human diagnosis

All FDG-PET/CT images were retrospectively reviewed by one experienced reader (12 years of experience with oncologic FDG-PET/CT; referred to as clinician A hereinafter) and one reader (2 years of experience with oncologic FDG-PET/CT; referred to as clinician B hereinafter), both of whom had no knowledge of the other imaging results or clinical and histopathologic data other than the presence of breast cancer. Because several groups have reported that the diagnostic performances of qualitative and quantitative assessments were not significantly different [9,12,13], we used a qualitative assessment in this study. The diagnostic certainty of assessing axillary LN metastasis was visually graded as 1 (definitely absent), 2 (probably absent), 3 (indeterminate), 4 (probably present), and 5 (definitely present). An LN was graded as 4 or 5 if it showed ^{18}F-FDG uptake greater than that of the reference background. A non-elevated PET signal or one considered compatible with physiological lymphatic uptake was rated as grade 1 or 2.

AI diagnosis

DCNNs, which have been the most popular AI model in recent years, have enabled tremendous achievements in various medical image analysis tasks [14]. However, the task in the present study is quite different from the previous tasks handled with DCNNs. In general-diagnosis tasks of medical images, DCNNs are usually trained to distinguish abnormality from normality by recognizing one specific type of lesion. In our present investigation, the objects of interest are patients diagnosed as having breast cancer, which requires the DCNN model to distinguish between breast cancer and axillary LN metastasis. DCNN models are faced with a dilemma in such a task since breast cancer and axillary LN metastasis have similar characteristics in terms of FDG uptake on PET images. In addition, in CT images, the anatomical structures of breast cancer and axillary LN metastasis are ambiguous to DCNN models without a human's technical knowledge. It is thus a challenging task for DCNN models to diagnose axillary LN metastasis with PET/CT images.

To overcome this problem, we designed a deep 3D residual convolutional neural network (CNN) equipped with an attention mechanism. The residual network is one of the most significant CNN structures and has been considered to be generally effective [15]. A

3D CNN can analyze PET/CT images without a deficiency of spatial information, which occurs with a general 2D CNN. The attention mechanism also enables the network to pay closer attention to regions that are truly meaningful to diagnoses, i.e., the locations at which the breast cancer and axillary LN metastases appear [16].

We constructed the network to perform a three-class classification: (1) no breast cancer, (2) breast cancer but no axillary LN metastasis, and (3) axillary LN metastasis of breast cancer. The network receives only the chest regions of the PET/CT images as inputs rather than the whole-body PET/CT images. The PET image and the CT image are concatenated as different channels to be fed into the network. One side of each PET/CT image (left chest or right chest; separated by the central line) is regarded as one training sample, which eliminates the need for healthy control subjects, since a side with no breast cancer can be used as a healthy side. In this manner, a total of 814 samples were obtained from the 407 patients with breast cancer: 400 normal samples, 210 breast cancer samples with no axillary LN metastasis, and 204 axillary LN metastasis samples. The three-class classification network was trained with the 814 samples.

Before the network was trained, the samples were normalized for more accurate and faster processing by the network. The PET images were clipped by using a maximum standardized uptake value (SUVmax) cutoff of 6, i.e., voxels with an SUV value >6 were assigned 6, and then normalized to [0, 1]. Similarly, the CT images were clipped by a low Hounsfield unit (HU) cutoff of −100 and a high HU cutoff of 200 and then normalized to [0, 1]. The cutoff values for the PET images and the CT images were determined by joint empirical and experimental estimations.

The AI-assisted diagnoses

To use the AI model as an assistant, we blended the diagnoses from the AI model with the clinicians' diagnoses. Since the AI model is not as reliable as the clinicians due to the limited amount of training data, the blending was biased towards the clinicians. Specifically, the graded clinicians' diagnoses were first converted into diagnostic probabilities of having axillary LN metastasis according to the diagnostic certainty: grade 1 corresponds to 0%, grade 2 to 25%, grade 3 to 50%, grade 4 to 75%, and grade 5 to 100%. The diagnostic probability from the clinicians (which we refer to as $\square_{\square\square\square}$) was then blended with the diagnostic probability from the AI model (which we refer to as $\square_{\square\square}$) using a confidence weight $\alpha = \square\square\square\ (\square_{\square\square\square}, 1 - \square_{\square\square\square})$ as the following equation:

$$\square_{\square\square\square\square\square} = \square \times \square_{\square\square\square} + (1 - \square) \times \square_{\square\square}.$$

Finally, the blend diagnostic probability was converted back into the graded diagnosis in the following manner: probabilities of 0%–20% are regarded as grade 1, 21%–40% as grade 2, 41%–60% as grade 3, 61%–80% as grade 4, and 81%–100% as grade 5.

Based on a generally valid assumption in the field of deep-learning that predictions with high confidence made by DCNN models tend to be more accurate than those with low confidence, we did not adopt diagnoses with relatively low confidence from the AI model for the AI-assisted diagnosis in this study. Here, 'confidence' denotes $\square\square\square\ (\square_{\square\square}, 1 - \square_{\square\square})$. To determine an appropriate confidence threshold, we studied the relationship between the threshold and the ratio of predictions with a confidence value larger than the threshold on the 414 samples with breast cancers. From Figure 1 illustrating the relationship, it can be seen that the ratio decreases slowly until the threshold increases to around 0.95, and then the ratio decreases much faster. We therefore chose 0.95 as the confidence threshold in this study.

In the AI-assisted diagnosis system, we can quantify how the AI assistance impacts a clinician's diagnoses as follows. For diagnoses of grade 1 and grade 5, the AI assistance has no effect since the confidence weight α is 1. For diagnoses of grade 2 and grade 4, the AI model can either agree with the clinician and enhance the diagnostic certainty, i.e., modify the grade to 1 or 5, or query the clinician's diagnosis and modify the grade to 3. For diagnoses of grade 3, the AI model can help the clinician to make to some extent definite diagnoses and modify the grade to 2 or 4. Note that these cases are limited to samples selected by the confidence threshold. The AI diagnoses screened out by the threshold are not taken into consideration, and thus the clinician's diagnoses are considered the final diagnoses for these samples.

Statistical analyses

A five-fold cross-validation was conducted on the 407 patients. For the AI model, a receiver operating characteristic (ROC) curve and an area under curve (AUC) value of the ROC curve were calculated for evaluation since the diagnoses from the AI model are continuous probabilities. However, the diagnoses from the two clinicians are of five grades so that it is less meaningful to compare the ROC curves between the clinicians and the AI model. To compare the performances of the AI model and the clinicians and evaluate the performance of the AI-assisted diagnosis, we used sensitivity, specificity and accuracy as evaluation metrics.

Results

The evaluations were performed mainly on the 414 samples of the half-chests with breast cancers. The performances of the human (clinicians') diagnoses, AI diagnoses and AI-assisted diagnoses are presented as follows. Some supplementary results are also provided for further analysis.

Human diagnoses

In general, LNs graded as 4 and 5 are considered positive, and on the 414 samples, the side-based sensitivity, specificity, and accuracy values of clinician A's reading for diagnosing axillary LN metastasis were 59.8% (122/204), 99.0% (208/210) and 79.7% (330/414), respectively. When including LNs of grade 3 as positive, the side-based sensitivity, specificity and accuracy of clinician A's reading were 74.0% (151/204), 96.7% (203/210) and 85.5% (354/414), respectively.

For clinician B, on the 414 samples, the side-based sensitivity, specificity, and accuracy when grade 4 and 5 were considered positive were slightly lower than the results of clinician A, at 57.4% (117/204), 99.5% (209/210), and 78.7% (326/414), respectively. The side-based sensitivity, specificity, and accuracy when grades 3, 4, and 5 were considered positive were 68.6% (140/204), 99.0% (208/210), and 84.1% (348/414), respectively.

AI diagnosis

For the 414 samples, the side-based AUC of the AI diagnosis for axillary LN metastasis was 0.868. The ROC curve is shown in Figure 2. The maximum Youden's index (J = sensitivity + specificity − 1) is marked on the curve. The side-based sensitivity, specificity, and accuracy values at the maximum Youden's index were 73.5% (150/204), 89.0% (187/204), and 81.4% (337/414), respectively.

AI-assisted diagnosis

Table 3 compares the performances of the human diagnoses and AI-assisted diagnoses for axillary LN metastasis on the 414 samples. The AI-assisted diagnosis results were obtained by the aforementioned blending method in which the diagnoses of grades 2, 3, and 4 from the clinicians may be modified by the AI model. The side-based values of sensitivity, specificity, and accuracy of the two clinicians with and without AI assistance under different positive standards are listed in the Table to demonstrate the effect of AI assistance.

As shown in Table 3, when considering grades 4 and 5 as positive, the AI assistance brought significant improvements in sensitivity and accuracy while keeping the extremely high specificity value unchanged. The two clinicians' sensitivities were increased by 8.8% and 6.8% and the accuracies were increased by 4.4% and 3.4%, respectively. These improvements indicate that the AI assistance helped the clinicians make relatively accurate diagnoses for the ambiguous samples graded as 3 by the clinicians. When considering only grade 5 as positive, the diagnoses of the clinicians were also improved considerably by the AI assistance in sensitivity (increased by 17.6% and 20.6% respectively) and accuracy (increased by 8.4% and 10.1% respectively). The improvements were gained by enhancing the diagnostic certainty with the AI assistance. However, when considering grades 3, 4, and 5 as positive, the AI assistance hardly affected the clinicians' performances. This result implies that the AI model cannot accurately diagnose the positive samples graded as 2 by the clinicians and cannot recognize more negative samples than the clinicians. As a whole, according to Table 3, the effects of the AI assistance on the two clinicians were substantially consistent.

Table 4 and Table 5 elaborate the effect of AI assistance on the diagnoses made by the two clinicians, i.e., which grades the samples were considered by the clinicians and reconsidered with AI assistance. Samples graded as 1 and 5 by the clinicians were not included in the tables since grades of these samples were unaffected. In the tables, a number marked by the asterisk '*' denotes diagnoses corrected by the AI assistance including (1) false-positive and false-negative samples reconsidered as grade 3, and (2) samples of grade 3 reconsidered correctly as grade 2 or grade 4. In contrast, a number marked '**' denotes mistakenly reconsidered diagnoses including (1) true-positive and true-negative samples reconsidered as grade 3, and (2) grade 3 samples reconsidered mistakenly as grade 2 or grade 4. It is clear in Tables 4 and 5 that the major contribution of the AI assistance came from helping the clinicians diagnose the ambiguous grade 3 samples.

Supplementary results

For a further evaluation the AI diagnoses and the AI-assisted diagnoses, some supplementary results are provided as follows. First, we observed an effect of the various PET/CT scanners on the diagnostic accuracy of the AI model. We divided the four PET/CT scanners used in this study into two groups based on the imaging quality that they provide. The Gemini GXL scanner (which has imaging quality inferior to the other scanners) comprised one group, and the other three scanners comprised the other group. The side-based ROC curves of AI diagnosis for the two groups are shown in Figure 3. The AUC values of the two ROC curves were 0.887 for the Gemini GXL and 0.826 for the other scanners. Our unexpected finding that the diagnoses obtained with the inferior scanner were more accurate may be explained by the biased data. Since 283 examinations of the total 407 FDG-PET/CT examinations were performed using the Gemini GXL scanner, the training of the AI model was biased toward the samples of the dominant scanner so that it underperformed on the other samples.

Considering the different environments of the two sides of the chest, especially in PET images, we also evaluated the AI diagnosis on each side. Figure 4 shows the side-based

ROC curves of which the AUC values were 0.891 (left side) and 0.852 (right side). The results seemed again unexpected because the performance on the left side (in which the uptake values in the heart region may produce a disturbance) were expected to be not better than that on the right side. We do not have a plausible explanation for this result; moreover, the results of 414 samples were not statistically meaningful enough.

The effect of AI assistance on the diagnostic performance depended on the performance of AI diagnosis on samples graded as 2, 3, and 4 by the clinicians. The side-based AUCs of the AI diagnoses on samples correctly graded as 2 or 4 by clinician A and samples graded as 3 by clinician A were 0.923 and 0.903, respectively, which were clearly better than the side-based AUCs for all 414 samples. These results explained why the AI assistance improved the diagnostic performance.

Finally, we provide some results of 814 samples including both sides of the 407 patients in Table 6. With the introduction of the 400 negative samples without breast cancer, the AI assistance showed a further contribution to specificity compared to the results obtained with 414 samples.

Discussion

FDG-PET/CT can be a noninvasive means for diagnosing LN metastasis. It imposes less burden on patients than invasive means such as SLNB and ALND. However, despite the very high specificities (99.0% and 99.5%) of FDG-PET/CT observed in this study, the sensitivities of the human diagnosis with FDG-PET/CT for axillary LN metastasis were quite poor (59.8% and 57.4%). Similar results have been reported by other groups [3–9]. To improve the sensitivity, we constructed an AI-assisted diagnosis system. In the system, an AI model was trained to diagnose axillary LN metastasis with PET/CT images. The AI model underperformed the two clinicians, whereas with a collaboration method, the AI model helped the clinicians as an assistant to improve the diagnostic accuracy. Such assistance may be promising in clinical applications of AI [17].

Our present findings demonstrated that the proposed AI-assisted diagnosis system contributed mainly to diagnoses for ambiguous cases graded as 3 by the clinicians. As shown in Tables 4 and 5, 24/34 and 15/24 samples of grade 3 were diagnosed correctly with the AI assistance, whereas there were relatively small numbers of incorrect diagnoses at 3/34 and 4/24. For the grade 2 and grade 4 samples, the AI assistance could query the human diagnoses, but it failed to improve the diagnostic accuracy.

On the other hand, the AI assistance also helped the clinicians enhance the diagnostic certainty of their diagnoses of grades 2 and 4, which was confirmed by the results, but such assistance may not truly affect the clinical diagnostic accuracy. For the grade 1 and grade 5 samples, we did not use the AI diagnosis because we observed that doing so reduced the diagnostic accuracy. In short, our present results indicate that samples that the clinicians mistakenly diagnosed were also difficult for the AI model — especially the numerous false negatives.

Nevertheless, there were still some false-negative diagnoses that were made by the clinicians and queried by the AI model. Figure 5 shows a false-negative sample diagnosed by clinician A. The clinician gave grade 2, whereas the AI model gave a positive diagnosis. As a result, the diagnosis was modified to grade 3 by the AI-assisted diagnosis system. The patient whose case is illustrated in Figure 5 was a 67-year-old woman with a Luminal B (HER2-negative)-type invasive ductal carcinoma (solid ductal cancer, ER 100%, PR 90%, HER2 1+, Ki-67 20%, grade 1, T2N1M0, stage IIB) and ipsilateral axillary LN metastasis diagnosed by aspiration cytology. After neoadjuvant chemotherapy, she received breast-conserving surgery including an SLNB and ALND.

In light of the limited number of patients used to train the AI model in this study, a larger contribution of AI assistance may be promising if a greater number of patients is made available for training AI models. This is also implied by the results on the two scanner groups shown in Figure 3. The performance of the AI diagnosis was much better for the group examined with the Gemini GXL compared to the group examined by the Gemini TF, Ingenuity TF or Discovery IQ5 due to the biased distribution of examination scanners. In cases of well-distributed examination scanners, we speculate that the performance of the AI diagnosis on the group of three scanners would not be worse than that for the Gemini GXL since the former scanners have better imaging quality than the Gemini GXL.

Due to limited performances and some other issues [18], AI cannot replace human clinicians completely in most clinical diagnoses. However, AI assistance can be useful in saving clinicians' time and/or improving diagnostic performance [19]. In the present study, the AI model which underperformed the clinicians showed an ability to diagnose cases that the clinicians considered indeterminate, with an AUC value of 0.903. This performance was even better than that on all of the samples, which indicates that the AI model has a different perspective from clinicians for diagnoses or can perceive some minute details. Such AI assistance may be desirable despite the difficulty in comprehensively interpreting how AI models make diagnoses.

Our study has several limitations, including its retrospective design, which may limit the generalization of the derived conclusions and may have caused statistical errors. Moreover, although a node-by-node-based analysis is ideal, it was difficult to correlate any given LN depicted by imaging with the same node in a dissection specimen. Therefore, the correlation between imaging results and pathological findings based on a side may be more reasonable for this type of study. In addition, as mentioned above, it was difficult to interpret the inference process of the AI model, which may hinder the AI model from gaining more trust. Although some approaches have been proposed to locate the regions that have the greatest impacts on AI's decisions [20,21], we observed herein that the localization can hardly be precise and thus gave poor hints. The best collaboration method between AI and clinicians merits further consideration and should be validated on a larger dataset.

Conclusion

Although the AI model trained in this study cannot outperform clinicians, the proposed AI-assisted diagnosis system can improve the diagnostic accuracy of human diagnosis mainly by assisting in the diagnoses of indeterminate patients. However, for hard false negatives, the AI model provides poor assistance. Future studies with more sufficient and well-distributed data may be informative and further improve the diagnostic performance.

Abbreviations

ALND: axillary lymph node dissection

AUC: area under curve

DCNN: deep convolutional neural network

ER: endocrine receptor

FDG-PET/CT: ^{18}F-fluorodeoxyglucose positron emission tomography/computed tomography

HER2: human epidermal growth factor receptor 2

HU: Hounsfield unit

LN: lymph node

NAC: neoadjuvant chemotherapy

ROC: receiver operating characteristic

SLNB: sentinel lymph node biopsy

SUVmax: maximum standard uptake value

TNM: tumor-node-metastasis

Ethics approval and consent to participate: The ethics committees of the institutions from which the patient population was drawn each provide approval for this study. The requirement for patients' informed consent was waived in light of the retrospective nature of the study.

Consent for publication: The requirement for patients' consent for publication was waived in light of the retrospective nature of the study.

Availability of data and material: The corresponding author can be contacted for requests regarding the data and material.

Competing interests: The authors declare that they have no competing interests.

Funding: This study was supported in part by the JSPS KAKENHI under grants JP17H01744, JP20K19857, and JP20K08015.

Authors' contributions

ZL was involved in the design of the study, designed and trained the AI model, analyzed the results, and was a main contributor to the manuscript. K. Kitajima was involved in the design of the study, collected and analyzed data, and was a main contributor to the manuscript. KH and RT were involved in the design of the study, helped with the analyses, and critically contributed to the manuscript. JT contributed to the data analysis. YM, K. Kudo, TO and MH critically contributed to the manuscript and coordinated the study. All authors read and approved the final manuscript.

Acknowledgements

None

References

1. Siegel, RL, Miller KD, Jemal A. Cancer statistics, 2019. CA Cancer J Clin 2019; 69: 7-34. doi: 10.3322/caac.21551.

2. Arriagada R, Le NG, Dunant A, Tubiana M, Contesso G. Twenty-five years of follow-up in patients with operable breast carcinoma: Correlation between clinicopathologic factors and the risk of death in each 5-year period. Cancer 2006;106:743-750. doi: 10.1002/cncr.21659.

3. Heusner TA, Kuemmel S, Hahn S, Koeninger A, Otterbach F, Hamami ME et al. Diagnostic value of full-dose FDG PET/CT for axillary lymph node staging in breast cancer patients. Eur J Nucl Med Mol Imaging 2009;36:1543-50. doi: 10.1007/s00259-009-1145-6.

4. Riegger C, Koeninger A, Hartung V, Otterbach F, Kimmig R, Forsting M et al. Comparison of the diagnostic value of FDG-PET/CT and axillary ultrasound for the

detection of lymph node metastases in breast cancer patients. Acta Radiologica 2012;53:1092-1098. doi: 10.1258/ar.2012.110635.

5. Liang X, Yu J, Wen B, Xie J, Cai Q, Yang Q. MRI and FDG-PET/CT based assessment of axillary lymph node metastasis in early breast cancer: A meta-analysis. Clin Radiol 2017;72:295-301. doi: 10.1016/j.crad.2016.12.001.

6. Song, Bong-Il, Hae Won Kim, and Kyoung Sook Won. Predictive value of 18 F-FDG PET/CT for axillary lymph node metastasis in invasive ductal breast cancer. Ann Surg Oncol 2017;24:2174-81. doi: 10.1245/s10434-017-5860-0.

7. Peare R, Staff RT, Heys SD. The use of FDG-PET in assessing axillary lymph node status in breast cancer: A systematic review and meta-analysis of the literature. Breast Cancer Res Treat 2010;123:281-290. doi: 10.1007/s10549-010-0771-9.

8. Robertson IJ, Hand F, Kell MR. FDG-PET/CT in the staging of local/regional metastases in breast cancer. The Breast 2011;20:491-4. doi: 10.1016/j.breast.2011.07.002.

9. Kitajima K, Fukushima K, Miyoshi Y, Katsuura T, Igarashi Y, Kawanaka Y et al. Diagnostic and prognostic value of 18 F-FDG PET/CT for axillary lymph node staging in patients with breast cancer. Jpn J Radiol 2016;34:220-8. 10.1007/s11604-015-0515-1.

10. Litjens G, Kooi T, Bejnord BE, Setio AAA, Ciompi F, Ghafoorian M et al. A survey on deep learning in medical image analysis. Med Image Anal 2017;4:60-88. doi: 10.1016/j.media.2017.07.005.

11. Wang H, Zhou Z, Li Y, Chen Z, Lu P, Wang W et al. Comparison of machine learning methods for classifying mediastinal lymph node metastasis of non-small cell lung cancer

from 18 F-FDG PET/CT images. EJNMMI Res 2017;7:11. doi: 10.1186/s13550-017-0260-9.

12. Wahl RL, Siegel BA, Coleman RE, Gatsonis CG. Prospective multicenter study of axillary nodal staging by positron emission tomography in breast cancer: a report of the staging breast cancer with PET Study Group. J Clin Oncol 2004;22:277-85.

13. Ueda S, Tsuda H, Asakawa H, Omata J, Fukatsu K, Kondo N et al. Utility of 18F-fluoro-deoxyglucose emission tomography/computed tomography fusion imaging (18F-FDG PET/CT) in combination with ultrasonography for axillary staging in primary breast cancer. BMC Cancer 2007;8:165. doi: 10.1186/1471-2407-8-165.

14. Shen D, Wu G, Suk H-I. Deep learning in medical image analysis. Annu Rev Biomed Eng 2017;19:221-48. doi: 10.1146/annurev-bioeng-071516-044442.

15. He K, Zhang X, Ren S, Sun J. Deep residual learning for image recognition. 2016 IEEE Conference on Computer Vision and Pattern Recognition (CVPR). doi: 10.1109/CVPR.2016.90.

16. Fukui H, Hirakawa T, Yamashita T, Fujiyoshi H. Attention branch network: Learning of attention mechanism for visual explanation. 2019 Proceedings of the IEEE Conference on Computer Vision and Pattern Recognition. 2019. arXiv: 1812.10025.

17. Asan O, Bayrak AE, Choudhury A. Artificial intelligence and human trust in healthcare: Focus on clinicians. J Med Internet Res 22.6 (2020): e15154. doi: 10.2196/15154.

18. Maddox TM, Rumsfeld JS, Payne PRO. Questions for artificial intelligence in health care. JAMA 321.1 (2019): 31-32. doi: 10.1001/jama.2018.18932

19. Jiang F, Jiang Y, Zhi H, Dong Y, Li H, Ma S et al. Artificial intelligence in healthcare: Past, present and future. Stroke Vasc Neurol 2.4 (2017): 230-243. doi: 10.1136/svn-2017-000101.

20. Zhou B, Khosla A, Lapedriza A, Oliva A, Torralba A. Learning deep features for discriminative localization. 2016 Proceedings of the IEEE Conference on Computer Vision and Pattern Recognition. 2016. arXiv:1512.04150.

21. Selvaraju RR, Cogswell M, Das A, Vedantam R, Parikh D, Batra D. Grad-CAM: Visual explanations from deep networks via gradient-based localization. Int J Comput Vis 2020:128;336-59. doi: 10.1007/s11263-019-01228-7.

Table 1. Patient and tumor characteristics

	n	**%**
Total patients	407	
Age mean (range)	59.2 (28–90)	
Tumor location, right/left/bilateral	228/172/7	56.0%/42.3%/1.7%
NAC, yes/no	125/282	30.7%/69.3%
Total breast cancers	414	
Type of surgery		
Breast-conserving surgery	164	39.6%
Modified radical mastectomy	250	61.4%
Histology		
IDC	373	90.1%
Others (Myxoid/ILC/apocrine/metaplastic)	15/14/11/1	0.9%
Molecular phenotype		

Luminal A (ER+/HER2−, Ki67 <20%)	148	35.7%
Luminal B (ER+/HER2−, Ki67 ≥20%)	120	29.0%
Luminal-HER2 (ER+/HER2+)	43	10.4%
HER2-positive (non-luminal)	43	10.4%
Triple-negative	60	14.5%
Axillary lymph node metastasis		
Present	204	49.3%
Absent	210	50.7%
Diagnostic tool of axillary node		
SLNB	197	47.6%
ALND	12	2.9%
SLNB and ALND	59	14.3%
Aspiration cytology and ALND	60	14.5%
Aspiration cytology and SLNB	19	4.6%
Aspiration cytology, SLNB, and ALND	67	16.2%
TNM Stage (I/II/III)	140/217/57	33.8%/52.4%/13.8%

ALND: axillary lymph node dissection, ER: endocrine receptor, HER: human epidermal growth factor receptor, IDC: invasive ductal cancer, ILC: invasive lobular cancer, NAC: neoadjuvant chemotherapy, SLNB: sentinel lymph node biopsy, TNM: tumor-node-metastasis.

Table 2. Clinical parameters of PET/CT scanners

Scanner	**Gemini GXL**	**Gemini TF64**	**IQ5**	**Ingenuity TF**
Vendor	**Philips**	**Philips**	**GE**	**Philips**
CT scanning				
Tube voltage	120 kV	120 kV	120 kV	120 kV
Effective tube	current auto-mA up to 120 mA	100 mA	12~390 mA (Smart mA: Noise Index 25)	100 mA (variable by Dose Right)
Detector configuration	16×1.5 mm	64×0.625 mm	16×1.25 mm	64×0.625 mm
Slice thickness, mm	2	2	3.75	2
Transverse FOV, mm	600	600	700	600
PET scanning				
FDG injection dose, MBq/kg	4	3	3.7	3.7
Scan time for each bed, mm	90	90	180	90
TOF	no	yes	no	yes
PET reconstruction				
Reconstruction	LOR-RAMLA	3D-OSEM	3D-OSEM+PSF+ Q-clear	3D-OSEM
Iterations	2	3	4	3
Subsets	n/a	33	12	33
Smoothing	n/a	n/a	Gaussian	n/a
FWHM of filter, mm			5	
Matrix	144×144	144×144	192×192	144×144
Pixel size, mm	4×4×4	4×4×4	3.125×3.125×3.125	4×4×4

FDG: fluorodeoxyglucose, FWHM: full-width at half maximum, LOR-RAMLA: line-of-response row-action maximum likelihood algorithm, OSEM: ordered-subset expectation maximization, PSF: point spread function, TOF: time of flight.

Table 3. The side-based sensitivity, specificity, and accuracy values of the human (clinicians') diagnoses and AI-assisted diagnoses on the 414 samples

Graded as positive	Clinicians with/without AI assistance	Sensitivity	Specificity	Accuracy
3, 4, 5	Clinician A w/o AI	74.0%	96.7%	85.5%
	Clinician A w/ AI	76.5%	94.3%	85.5%
	Clinician B w/o AI	68.6%	99.0%	84.1%
	Clinician B w/ AI	68.6%	99.0%	84.1%
4, 5	Clinician A w/o AI	59.8%	99.0%	79.7%
	Clinician A w/ AI	68.6%	99.0%	84.1%
	Clinician B w/o AI	57.4%	99.5%	78.7%
	Clinician B w/ AI	64.2%	99.5%	82.1%
5	Clinician A w/o AI	37.3%	100%	69.1%
	Clinician A w/ AI	54.9%	99.5%	77.5%
	Clinician B w/o AI	33.8%	100%	67.4%
	Clinician B w/ AI	54.4%	100%	77.5%

397

Table 4. Details of how the AI assistance affected the diagnoses made by clinician A

	Grade by clinician A					
Regraded with AI assistance	Grade 2 127		Grade 3 34		Grade 4 48	
	Positive 34	Negative 93	Positive 29	Negative 5	Positive 46	Negative 2
Grade 1	19	63				
Grade 2	7	22	3**	3*		
Grade 3	8*	8**	5	2	3**	
Grade 4			21*		7	1
Grade 5					36	1

Table 5. Details of how the AI assistance affected the diagnoses made by clinician B

Regraded with AI assistance	Grade by clinician B					
	Grade 2 12		Grade 3 24		Grade 4 49	
	Positive 8	Negative 4	Positive 23	Negative 1	Positive 48	Negative 1
Grade 1	2	2				
Grade 2	3	2	3**			
Grade 3	3*		5		1**	1*
Grade 4			15*	1**	5	
Grade 5					42	

Table 6. The side-based sensitivities, specificities and accuracies of human diagnosis and AI-assisted diagnosis on the 814 samples

Graded as positive	**Clinicians with/without AI assistance**	**Sensitivity**	**Specificity**	**Accuracy**
3, 4, 5	Clinician A w/o AI	74.0%	96.9%	91.2%
	Clinician A w/ AI	76.5%	97.0%	91.9%
4, 5	Clinician A w/o AI	59.8%	99.2%	89.3%
	Clinician A w/ AI	68.6%	99.3%	91.6%

Figure legends

Fig. 1. The relationship between the threshold and the ratio of predictions with a confidence value larger than the threshold on the 414 samples with breast cancers.

Fig. 2. The side-based ROC curve of the AI diagnosis for axillary LN metastasis on the 414 samples.

Fig. 3. The side-based ROC curves of AI diagnosis on samples of the two scanner groups.

Fig. 4. The side-based ROC curves of the AI diagnosis on two sides of the chest.

Fig. 5. A positive sample that clinician A graded as 2 (probably negative) and the AI model diagnosed as positive. **(a)** Maximum intensity projection (MIP) from FDG-PET. **(b)** Fused axial FDG-PET/CT showing moderate FDG uptake in the left breast tumor measuring 23 mm (*arrow*). **(c)** Axial FDG-PET. **(d)** Axial CT. **(e)** Fused FDG-PET/CT showing no abnormal FDG uptake in a left tiny (4-mm) axillary LN (*arrow*).

Figure 1

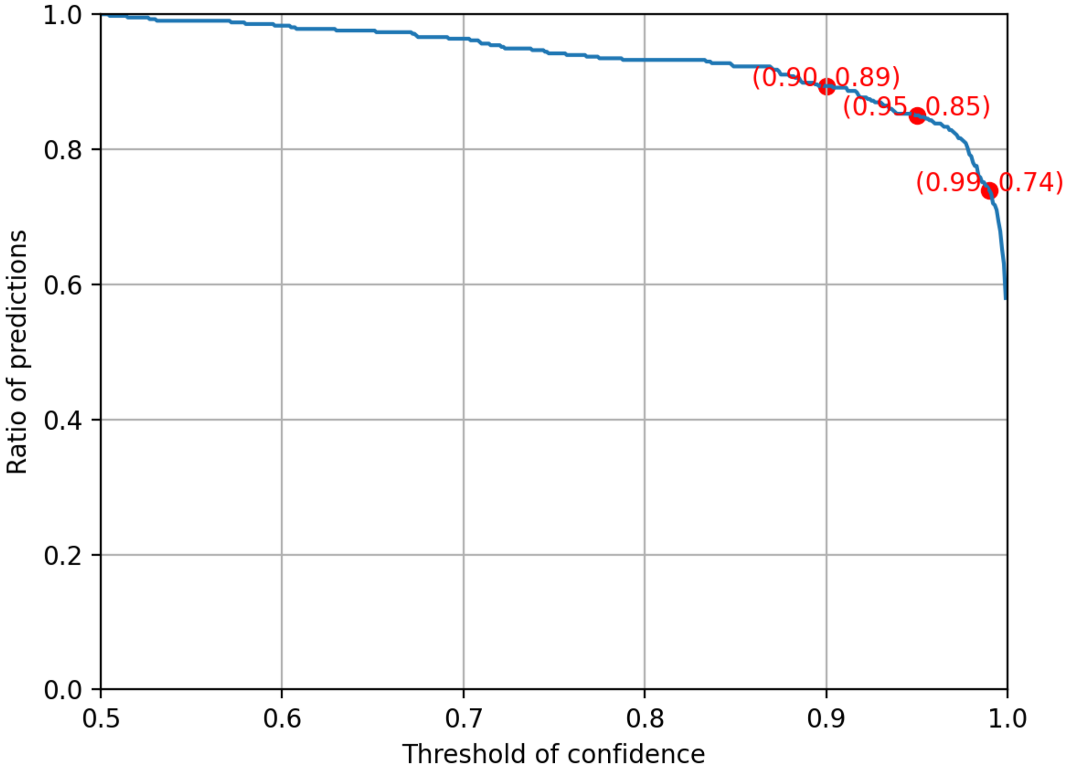
1.0
0.8
0.6
0.4
0.2
0.0
Ratio of predictions
0.5
0.6
0.7
0.8
0.9
1.0
Threshold of confidence
(0.90, 0.89)
(0.95, 0.85)
(0.99, 0.74)

Figure 2

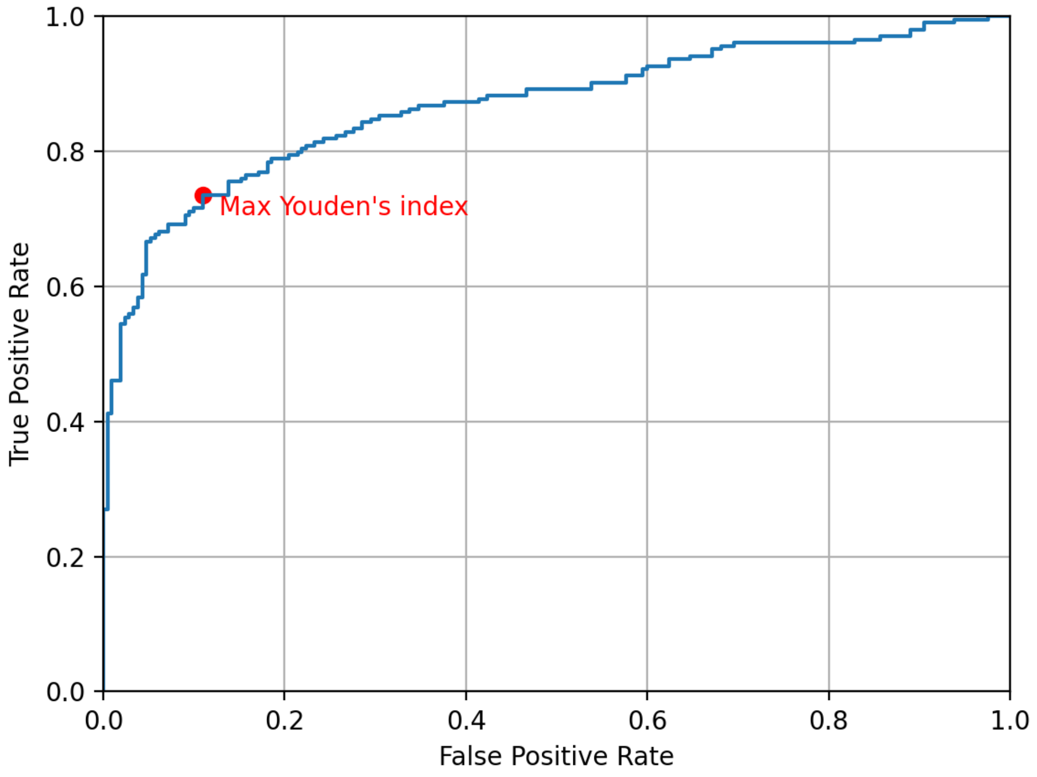
1.0
0.8
0.6
0.4
0.2
0.0
True Positive Rate
0.0
0.2
0.4
0.6
0.8
1.0
False Positive Rate
Max Youden's index

403

Figure 3

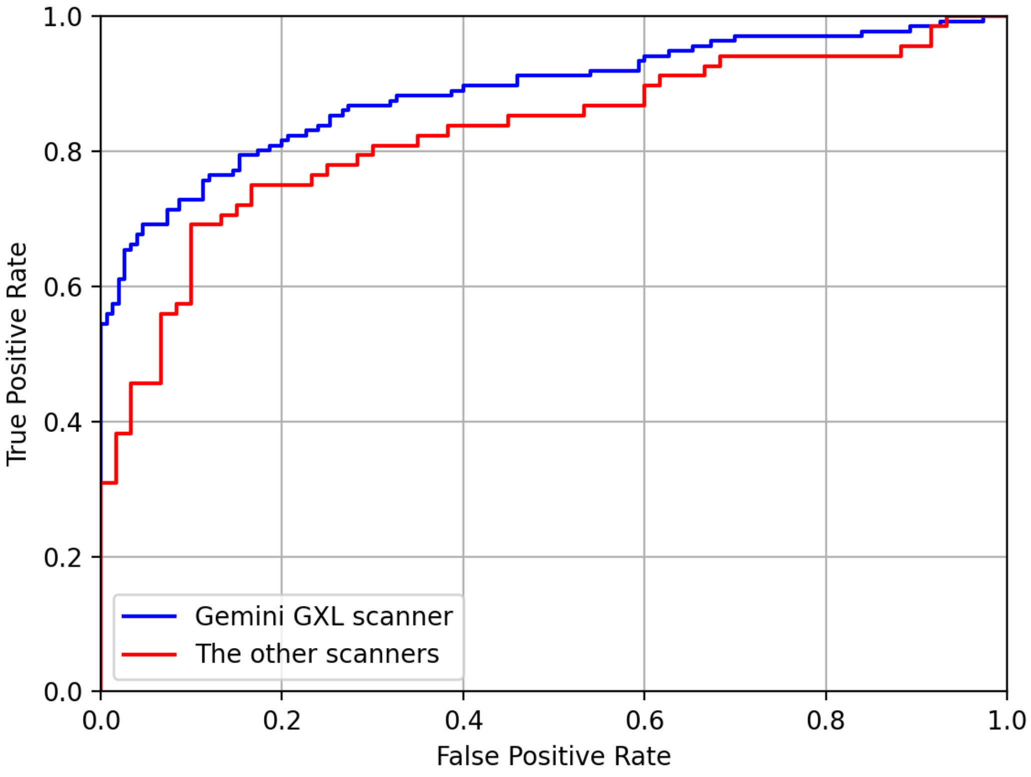
1.0
0.8
0.6
0.4
0.2
0.0
True Positive Rate
0.0
0.2
0.4
0.6
0.8
1.0
False Positive Rate
Gemini GXL scanner
The other scanners

404

Figure 4

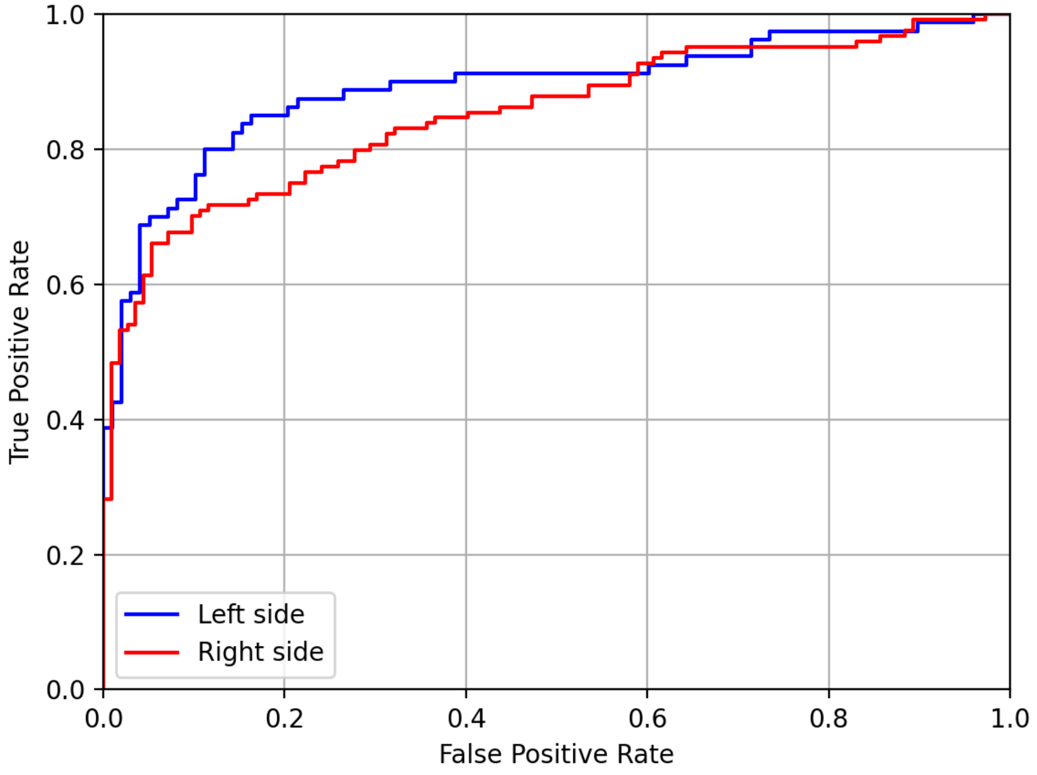
1.0
0.8
0.6
0.4
0.2
0.0
True Positive Rate
0.0
0.2
0.4
0.6
0.8
1.0
False Positive Rate
Left side
Right side

405

Figure 5

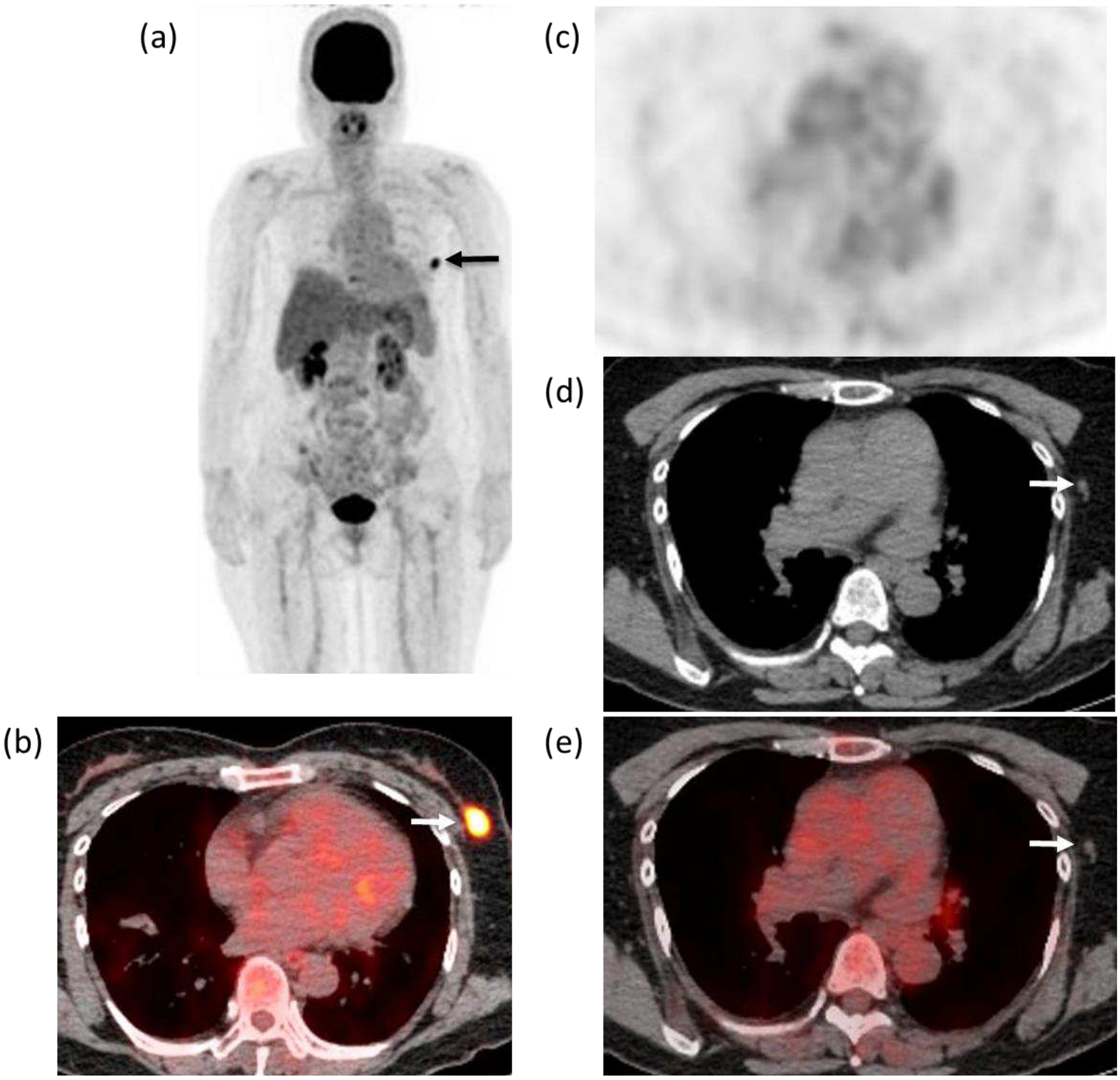

Figures

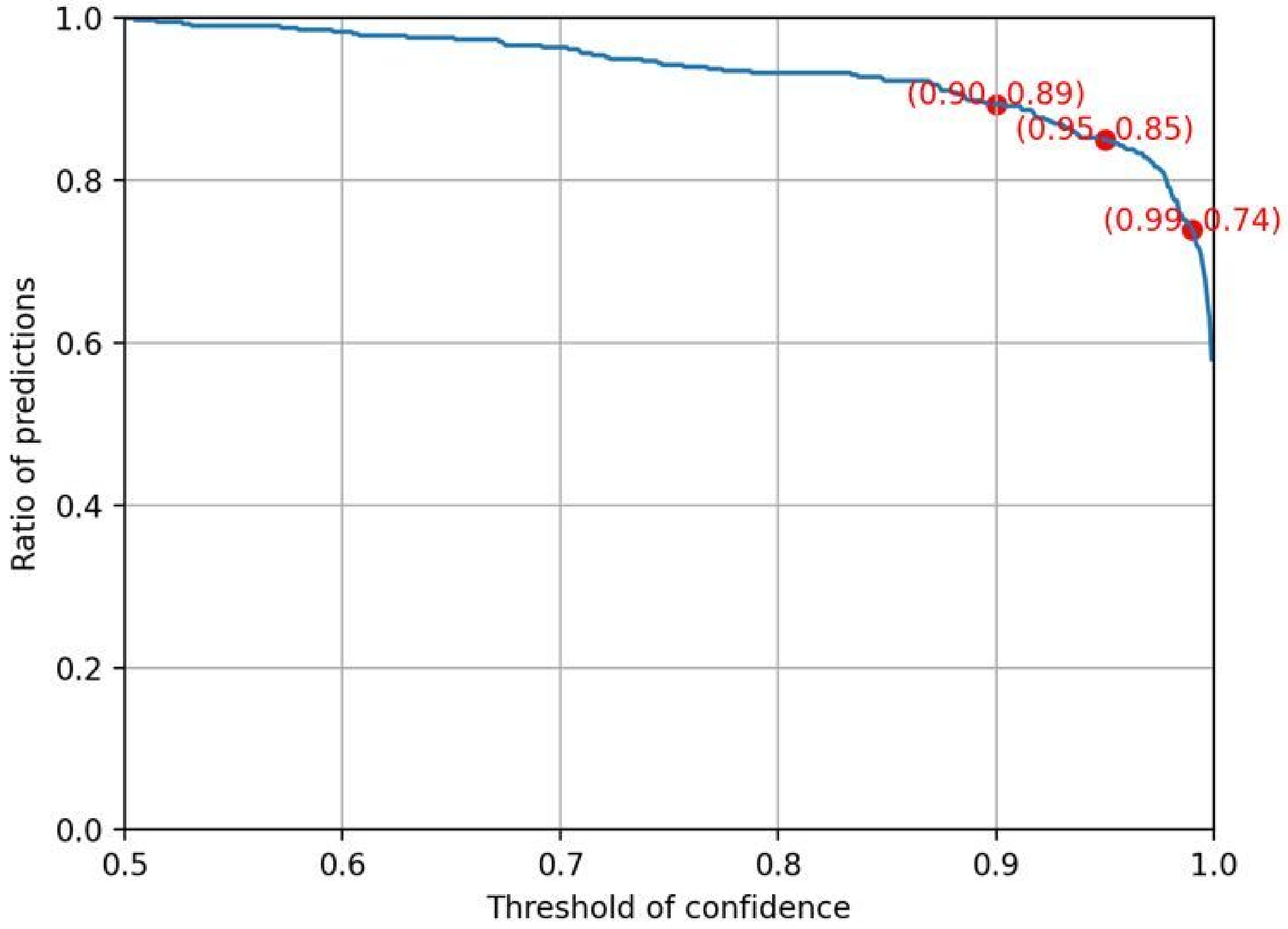

Figure 1

The relationship between the threshold and the ratio of predictions with a confidence value larger than the threshold on the 414 samples with breast cancers.

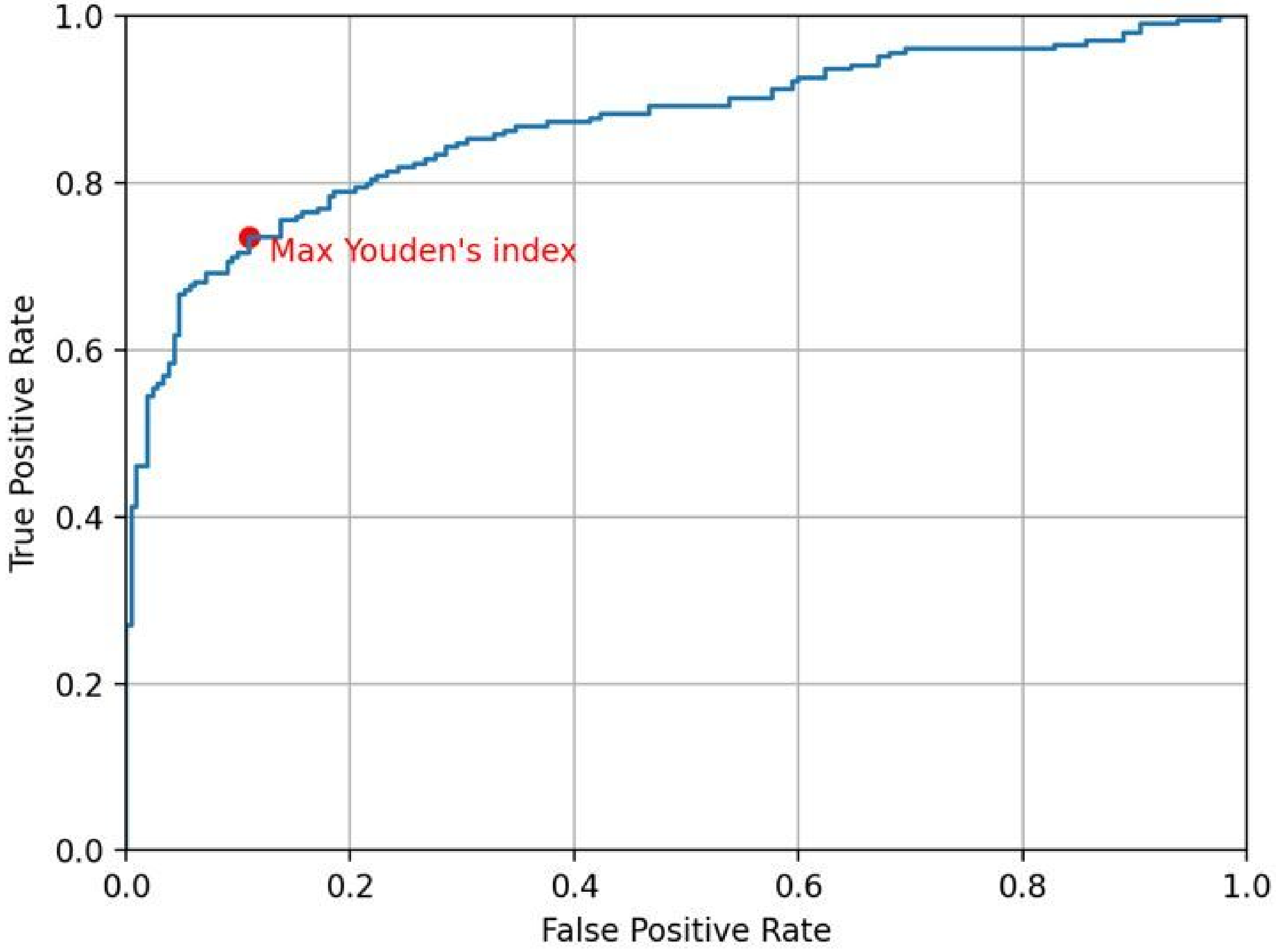

Figure 2

The side-based ROC curve of the AI diagnosis for axillary LN metastasis on the 414 samples.

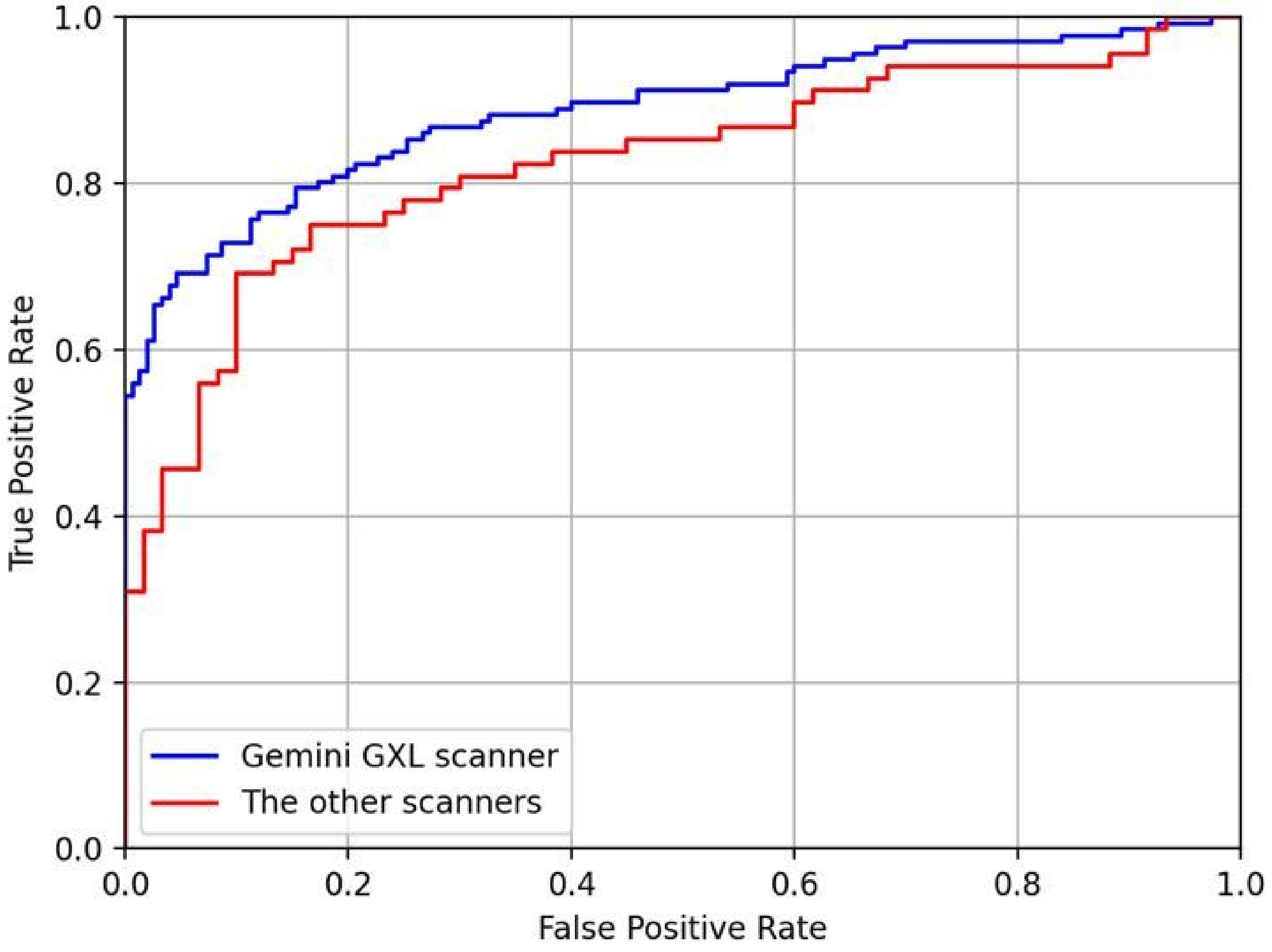

Figure 3

The side-based ROC curves of AI diagnosis on samples of the two scanner groups.

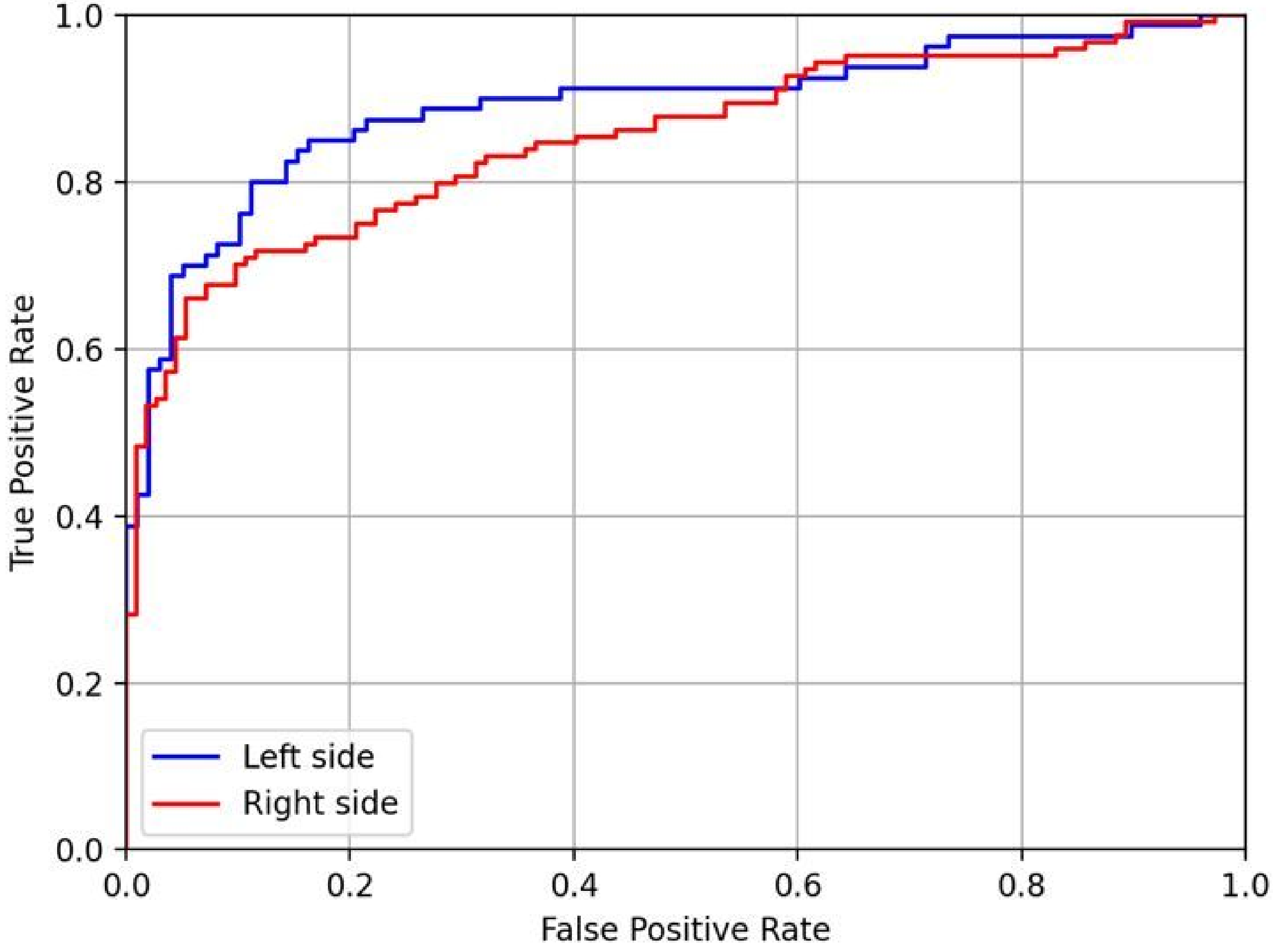

Figure 4

The side-based ROC curves of the AI diagnosis on two sides of the chest.

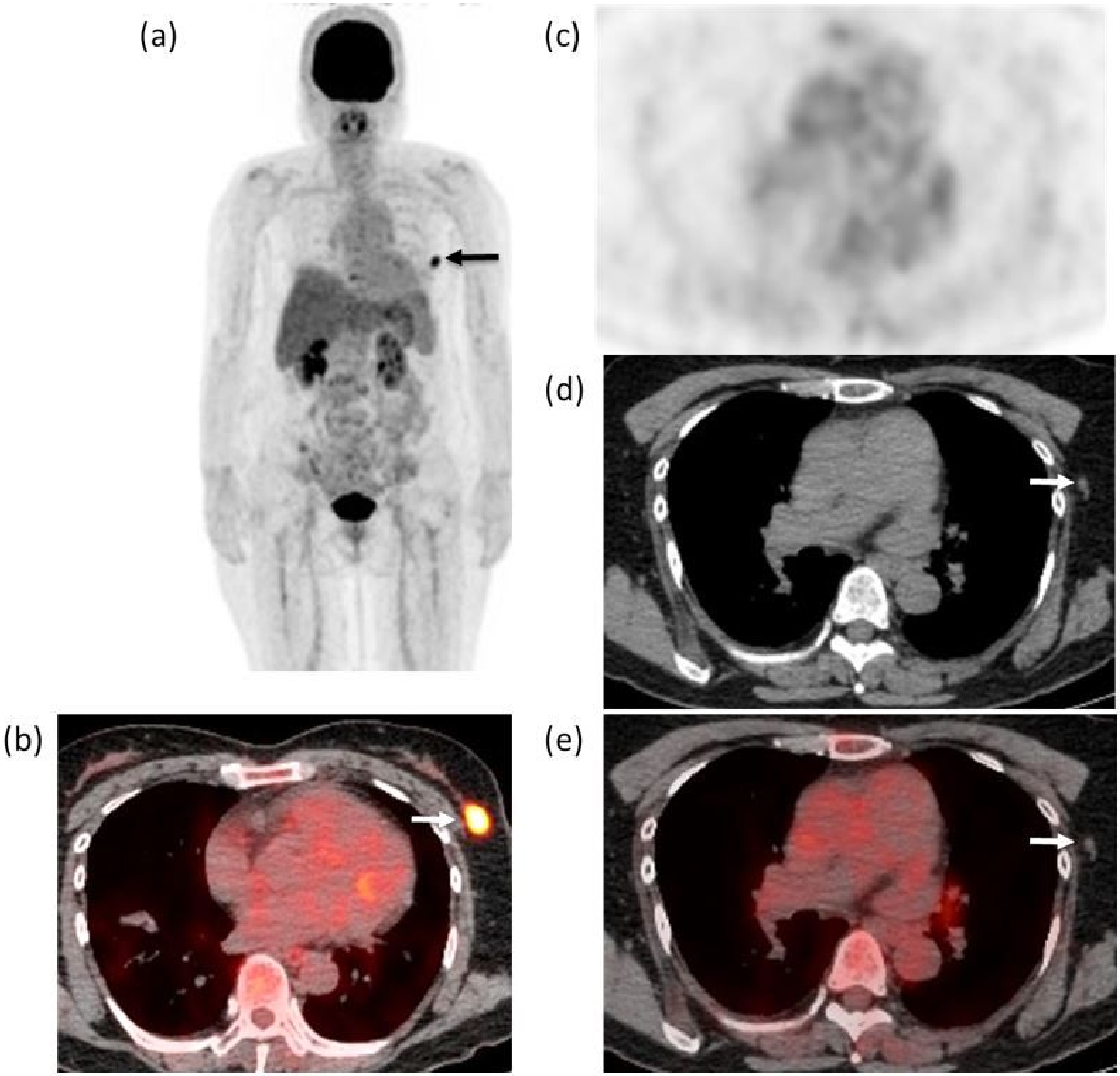

Figure 5

A positive sample that clinician A graded as 2 (probably negative) and the AI model diagnosed as positive. (a) Maximum intensity projection (MIP) from FDG-PET. (b) Fused axial FDG-PET/CT showing moderate FDG uptake in the left breast tumor measuring 23 mm (arrow). (c) Axial FDG-PET. (d) Axial CT. (e) Fused FDG-PET/CT showing no abnormal FDG uptake in a left tiny (4-mm) axillary LN (arrow).